Materials Science & Engineering A 771 (2020) 138614

Contents lists available at ScienceDirect

Materials Science & Engineering A

journal homepage: http://www.elsevier.com/locate/msea

Mechanisms of thermal cycling damage in polycrystalline Sn-rich solder joints

Marion Branch Kelly, Antony Kirubanandham, Nikhilesh Chawla *

Center for 4D Materials Science, Arizona State University, Tempe, AZ, 85287-6106, USA

ARTICLE INFO

Keywords:
Lead-free solder
Thermal aging
Thermal cycling
Grain boundary sliding
EBSD

ABSTRACT

Solder joints will experience elevated temperatures during operation due to resistive heating and ambient conditions. Device components have different thermal expansion characteristics, leading to straining of the solder joint and development of surface damage features. The anisotropic thermal expansion of βSn grains and discrepancy between the thermal expansion of intermetallic compounds causes degradation to be localized near grain boundaries and phase interfaces. Three experiments were conducted to investigate thermal effects on solder joint microstructure. Interrupted low temperature aging revealed the formation and movement of grain boundary ledges and uninterrupted thermal aging confirmed that the ledges formed during the cooling cycle of the experiment. Finally, high temperature thermal cycling demonstrated the acceleration of surface damage that accompanies an increase in peak temperature and cycling frequency. The orientation of the c-axis of the Sn matrix grains proved to be the critical feature controlling the direction of grain boundary ledge migration and type of surface deformation surrounding Cu_6Sn_5 intermetallic needles.

1. Introduction

Solder joints serve as electrical, mechanical and thermal connections in microelectronic packages [1,2]. With increasing package density, small solder bumps experience very high current densities that cause resistive heating and thermomechanical damage due to thermal expansion of multiple package components [3,4]. Due to its body centered tetragonal crystal structure, βSn exhibits anisotropic behavior where mechanical, thermal, electrical and diffusive properties are different along different crystallographic directions [5–10]. The thermal expansion of Sn along the c-axis is twice that along the a-axis [3,11], leading to strain concentrations along high angle grain boundaries [12]. This strain concentration can lead to grain boundary sliding, grain boundary delamination and recrystallization [4,12–17] depending on the temperature of testing, number of cycles and total testing time. The distribution of second phase particles can also have an effect on the degree of damage due to the ability of particles to pin grain boundaries and prevent recrystallization [12,18].

The evolution of Sn grains during thermomechanical fatigue (TMF) has been studied using *in situ* EBSD experiments [19–22]. While many thermal experiments have historically been postmortem analyses, a significant portion of history is lost using only this technique. In order to fully capture the evolution of solder joint microstructure, *in situ* testing and characterization techniques were adopted. *In situ* observations by Matin et al. were key in understanding the microstructural evolution under purely thermal and mechanical fatigue conditions [19]. Local stress concentrations were observed at the Cu/solder interface which were found to be imposed by sample constraints [19]. At high angle grain boundaries, the anisotropic expansion of Sn grains proved to be a dominant stress localization mechanism [19]. TMF studies done by Telang et al. found that recrystallization/grain growth mechanisms change the initial solder microstructure to an elastically compliant twinned structure [20]. These tests also resulted in the removal of small grains via annealing, resulting in a single orientation microstructure. Thermal cycling was also seen to induce formation of grain boundary ledges after recrystallization processes were complete [20]. Chen et al. investigated the *in situ* crystallographic evolution of SAC solder joints under different mechanical testing conditions [21]. The *in situ* observations were crucial in understanding how recrystallized grains evolve by sub-grain rotation and that these recrystallized zones are potential crack initiation sites as confirmed by their lower hardness values [22]. James et al. recently developed a custom *in situ* electromigration testing fixture and utilized lab-scale X-ray computed tomography to provide a volumetric description of the Cu–Sn intermetallic phases that formed

* Corresponding author.
E-mail address: nchawla@asu.edu (N. Chawla).

https://doi.org/10.1016/j.msea.2019.138614
Received 26 August 2019; Received in revised form 28 October 2019; Accepted 29 October 2019
Available online 1 November 2019

Table 1
Parameters used for High Temperature Thermal Cycling.

Parameter	Rate or Duration
Ramp Up/Down Rate	25 °C/min
Ramp Up/Down Time	5 min
Hold Time	25 min
Cycle Period	60 min

during current stressing [23]. The fixture was also utilized for EBSD analysis in order to measure the effective diffusivity and effective charge product, D_eZ^* of Cu in solder [24].

Although reports have suggested that a variety of degradation phenomena occur during thermal aging and thermal cycling, the evolution of specific damage features has not been thoroughly investigated and explained in the context of Sn grain orientation. The present work focuses on *in situ* characterization of thermal damage inside a scanning electron microscope (SEM) by studying the evolution of microstructural features such as Sn grain orientation, grain size and intermetallic compound (IMC) structure and morphology. Low temperature interrupted thermal aging was conducted for 120 h to characterize the initial stages of thermal damage on the solder joint surface. Electron backscatter diffraction (EBSD) analysis was done in conjunction with SEM imaging to elucidate the underlying mechanisms driving grain boundary ledge formation and migration. Uninterrupted thermal aging was done to study the relationship between heating and cooling cycles and ledge formation. High temperature thermal cycling was done to investigate the effect of increased operating temperature and cycle frequency on surface damage features.

2. Materials and experimental methods

2.1. Samples and testing fixtures

Samples used for this study were Cu-pure Sn–Cu sandwich joints, fabricated by reflowing Sn solder spheres (99.99% purity, Indium, Ithica N. Y.) between two polished oxygen free high conductivity Cu (OFHC) wires (5 N purity, ESPI Metals). Solder joints were prepared using Sn spheres and Cu wires with 500 μm diameters. The fabrication technique and reflow profile used are described elsewhere [25]. After reflow, the sandwich joints were mounted in pre-machined grooves on epoxy pucks using ethyl cyanoacrylate super glue. This enabled the solder joints to be polished and later removed by dissolving the super glue in a bath of acetone. The solder joints were mechanically polished, ending with a 0.05 colloidal silica solution, to ensure a good surface finish for SEM imaging and EBSD analysis. After polishing about halfway through the joint thickness, the samples were carefully removed and cleaned in acetone and isopropyl alcohol baths to ensure removal of all glue residue.

The solder joints were then mounted within a custom fixture designed for *in situ* thermal aging, electromigration (EM), EBSD analysis

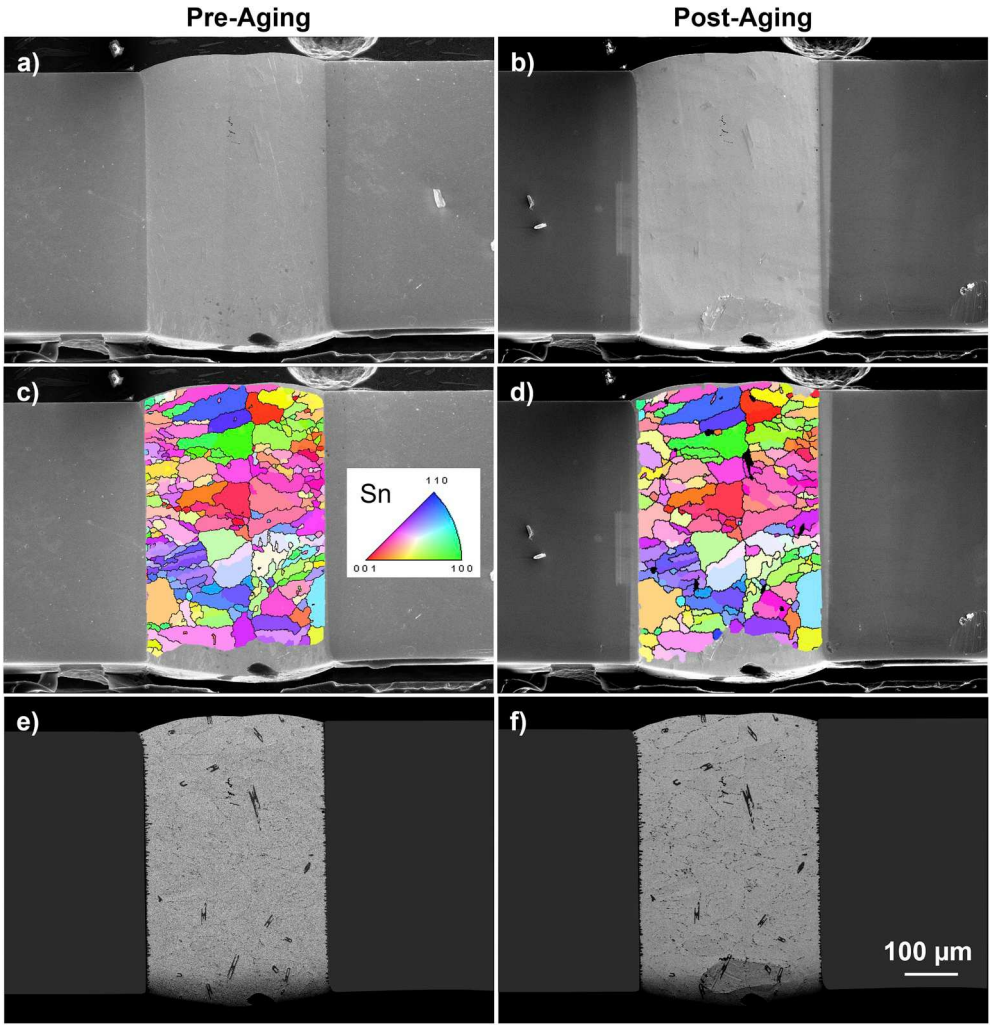

Fig. 1. (a,c,e) Pre and (b,d,f) post-aging images of the interrupted thermal aging sample: (a,b) SE SEM images, (c,d) SE images with OIM map overlaid and grain boundaries highlighted in black, and (e,f) BSE SEM images showing dark grey Cu_6Sn_5 IMC needles in the solder bulk.

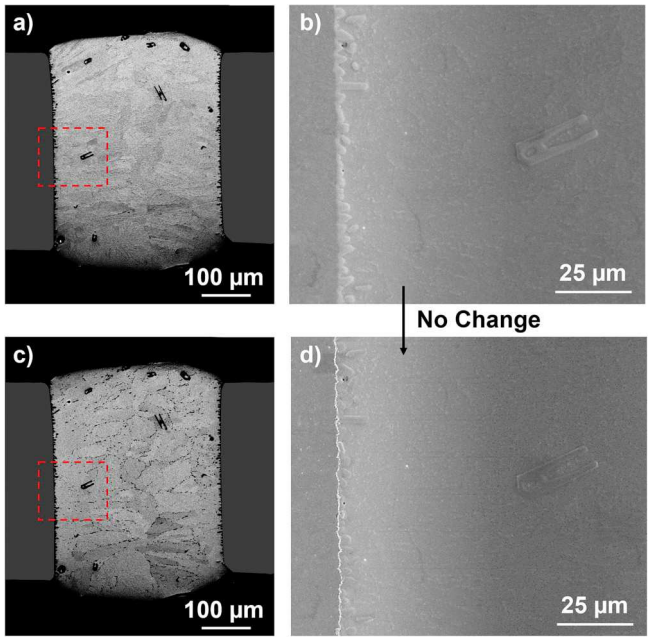

Fig. 2. (a,b) Pre and (c,d) post aging SEM images of uninterrupted thermal aging sample taken at 100 °C: (a,c) overall BSE image of the solder joint and (b, d) higher magnification SE images of the solder surface (indicated by red boxes in a and c) showing no change between the pre and post aged conditions. (For interpretation of the references to colour in this figure legend, the reader is referred to the Web version of this article.)

and X-ray computed tomography analysis. The details of this fixture are described elsewhere [23]. Samples mounted in the fixture remained undisturbed until the completion of each experiment. The sample fixture was mounted onto a programmable ceramic resistive heater (Watlow Electric Manufacturing Company, St. Louis, MO) that could heat samples up to 200 °C. The aluminum sample fixture possessed good thermal conductivity, ensuring efficient heat transfer and a stable sample temperature. Sample temperatures were recorded live during testing through the use of a LabVIEW (National Instruments, Austin, Texas) user interface.

2.2. Interrupted thermal aging

To study the microstructural effects of interrupted thermal aging, a 500 µm solder joint was fabricated, prepared according to the method in Section 2.1 and thermally aged *in situ* in the SEM. The sample was aged at 100 °C for 120 h, interrupted at 12-h increments to be cooled to room temperature (25 °C) for secondary electron (SE) and backscatter electron (BSE) imaging. This test could also be interpreted as low temperature thermal cycling with a peak hold temperature of 100 °C, 0.43 of the melting temperature of Sn ($T_{melt} = 232$ °C).

2.3. Uninterrupted thermal aging

A second 500 µm solder joint, fabricated similarly, was used for an *in situ* uninterrupted aging test. This test was done to confirm the effects of the thermal cycling imposed by the interruptions in the interrupted thermal aging experiment. In order to avoid the influence of heating and cooling cycles, the solder joint was held at 100 °C for SEM imaging which was done before and after a period of 120 h of aging.

2.4. High temperature thermal cycling

The final investigation in this work was on a 500 µm solder joint used to study the effect of high temperature thermal cycling on damage development. The sample was mounted in the *in situ* fixture and cycled between room temperature (25 °C) and 150 °C (0.65 T_{melt}) with a cycle time of 1 h. The sample was tested for a total of 118 cycles. Table 1 lists the test parameters used for thermal cycling. EBSD and SEM imaging was done before testing to characterize the initial microstructure and SEM images were taken periodically during testing to monitor the evolution of damage features on the sample surface.

3. Results

All experiments were conducted on polycrystalline solder joints with similar as-fabricated microstructures consisting of βSn grains with random sizes and orientations, randomly distributed Cu_6Sn_5 IMC needles and an even dispersion of fine Cu_6Sn_5 particles. Orientation imaging microscopy (OIM) was used to create grain orientation maps from EBSD analysis. These maps are included in the results where grain structure

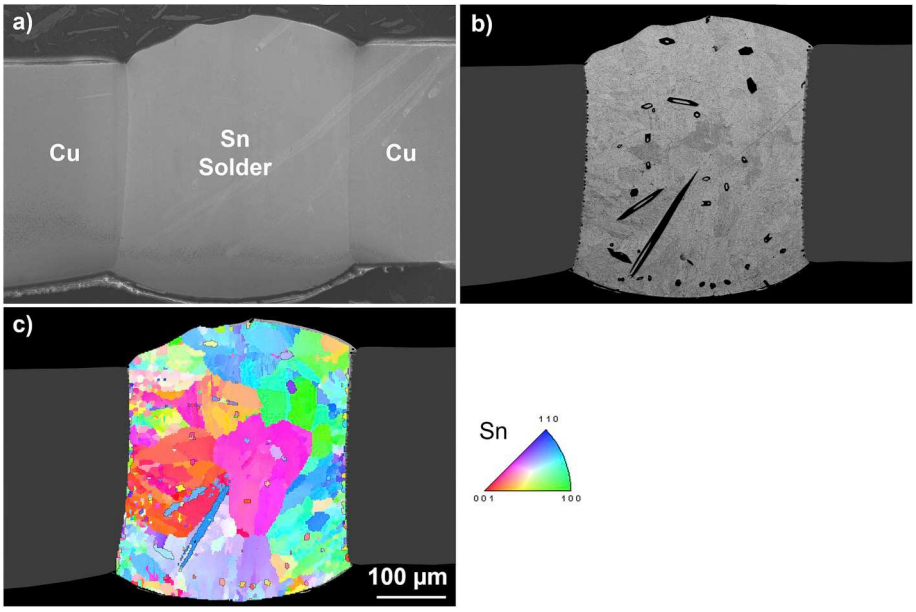

Fig. 3. As-fabricated SEM characterization of the thermal cycling solder joint: (a) SE image with Cu substrate wires and Sn solder region indicated, (b) BSE image showing Cu_6Sn_5 IMC needles in dark grey and (c) OIM map of the solder joint cross section.

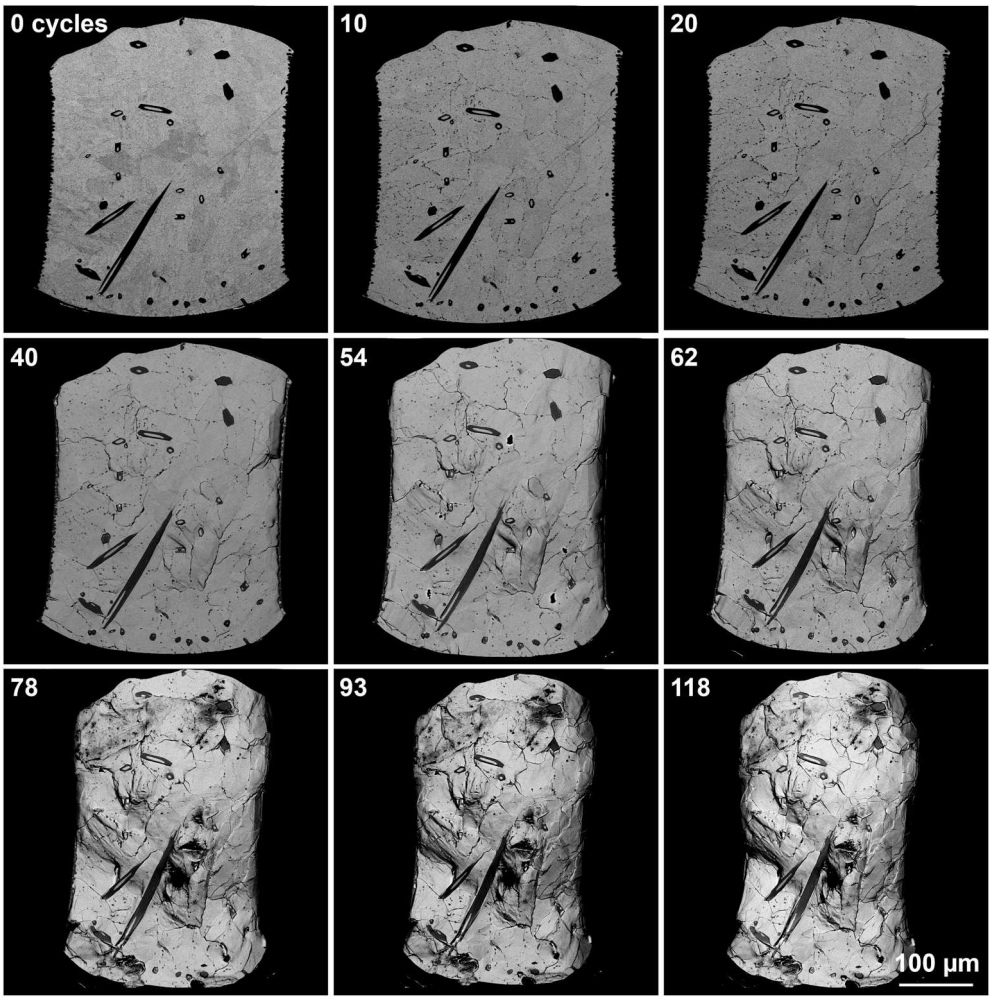

Fig. 4. BSE images of the thermally cycled sample, showing images from 0, 10, 20, 40, 54, 62, 78, 93, and 118 cycles. Surface relief is visible across the majority of the joint and appears concentrated along grain boundaries. Compression along the horizontal dimension of the joint is evident, causing the solder region to bulge outwards.

merits further discussion.

3.1. Interrupted thermal aging

The solder joint used for the interrupted aging experiment was characterized in the SEM before, after and at 11 time steps during testing. The initial and final sample surfaces are shown in Fig. 1. SEM images of the sample surface show no obvious signs of surface deformation, however higher resolution SEM images revealed the formation of ledges along high angle grain boundaries. OIM maps were taken at 12-h intervals during testing and showed constant grain size and grain boundary misorientation trends, indicating no grain growth or grain rotation took place during testing. The initial OIM map was nearly identical to the final.

3.2. Uninterrupted thermal aging

The solder joint used for the uninterrupted aging test was brought to its hold temperature of 100 °C inside the SEM, imaged, held for 120 h, and imaged again before cooling to room temperature. The initial and final sample surfaces are shown in Fig. 2. There was no detectable surface relief or deformation. Although high angle grain boundaries were present, no grain boundary sliding or ledge formation was observed.

3.3. High temperature thermal cycling

The sample selected for high temperature thermal cycling had a polycrystalline Sn grain structure with a random distribution of hexagonal Cu_6Sn_5 needles in the sample bulk, shown in Fig. 3. In contrast to the previous two samples, the thermally cycled sample contained large regions with similarly oriented Sn grains and a larger area fraction of IMC needles visible on the sample cross section. Sn grains with the a-axis or b-axis of the Sn lattice normal to the sample surface are shown in the OIM map in Fig. 3c as predominantly green or blue and grains with the c-axis normal to the sample surface are shown as predominantly red or pink. The sample's progressive surface deformation during thermal cycling is shown in Fig. 4. Surface deformation included grain boundary sliding along high angle grain boundaries, illustrated in Fig. 5, IMC needle push out or sink in and compression along the length of the solder joint. OIM mapping was not possible after the first 10 thermal cycles because the surface relief caused a large amount of error in the EBSD analysis. Although ledges visible on the solder surface after 118 cycles align with grain boundaries in the initial OIM map, the degree of deformation likely caused the Sn grains to recrystallize in the bulk of the joint.

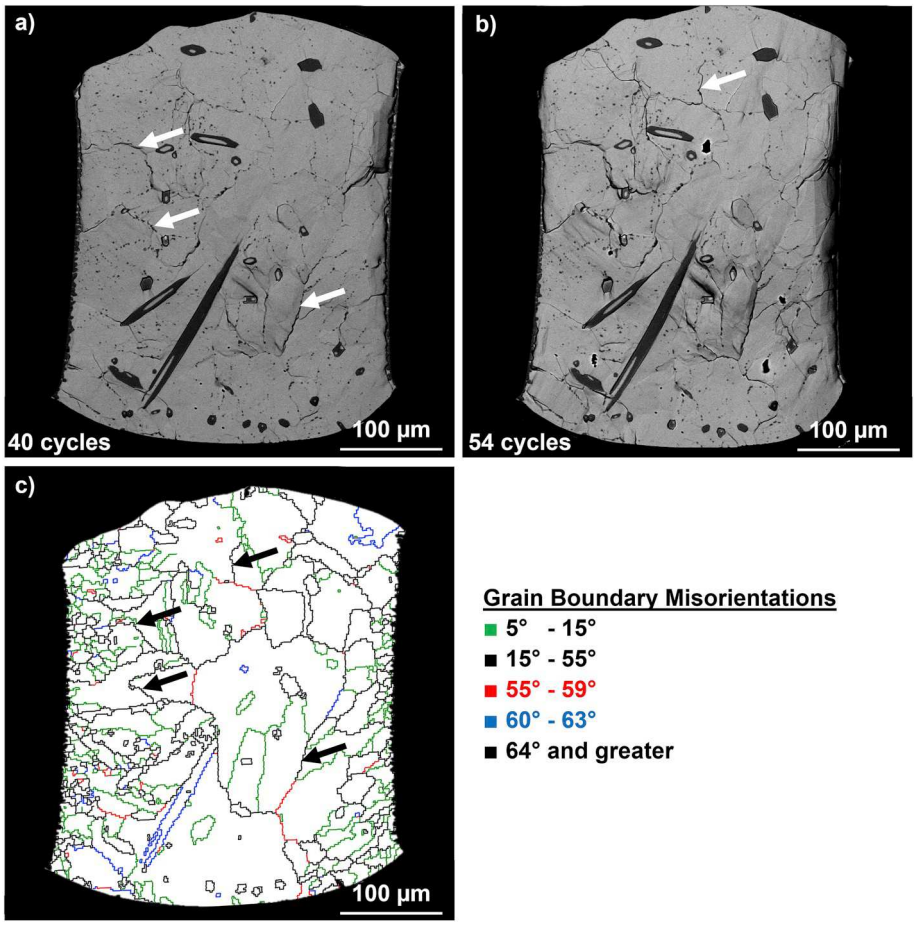

Fig. 5. BSE images of thermally cycled solder joint at (a) 40 and (b) 54 cycles when the sample began to show significant grain boundary sliding, indicated by the white arrows. Locating the incidences of grain boundary sliding from the SEM images (now in black arrows) on a (c) grain boundary map shows that grain boundary sliding occurred along high angle grain boundaries.

4. Discussion

4.1. Low temperature surface evolution

Both the interrupted and uninterrupted thermal aging experiments were done at 100 °C which is less than half the melting point of pure Sn. It was not unusual that neither solder joint experienced grain growth or recrystallization due to the low testing temperature and lack of applied external stress. No IMC growth took place at the solder-Cu wire interfaces or in the solder bulk and no Kirkendall voids were seen in the interfacial IMC layers. Kirkendall voiding is caused by a difference in diffusion rates between Cu and Sn, where Cu diffuses more rapidly than Sn through Cu–Sn IMCs [26]. Most solder studies that demonstrate Kirkendall void formation test samples for hundreds of hours at temperatures greater than 100 °C, making void formation in the low temperature thermal experiments unlikely [26–28]. In addition, the propensity for a solder joint to demonstrate Kirkendall voiding has been linked to the purity of the Cu substrate, where high purity Cu substrates reduce or eliminate voiding while less pure electroplated substrates demonstrate significant voiding [26,29]. Due to the low testing temperature and short timescale of these thermal experiments and the use of OFHC Cu wires, Cu diffusion was minimal and Kirkendall voids were not present.

Instead, the microstructural evolution was limited to the solder joint surface where ledges formed along high angle grain boundaries. Surface imaging of the interrupted aging sample revealed ledge formation at 24 h. Over time the ledges multiplied, forming banded structures as grain boundaries slid incrementally during each interruption. Fig. 6 shows high-resolution SEM images of one such banded region. A dashed line indicates the high angle grain boundary of interest. Where the grain boundary intersected with fine Cu_6Sn_5 IMC particles, the particles pinned the boundary and prevented it from further migration [30,31]. In a particle-free region the boundary was free to move and formed multiple ledges. At the end of the interrupted experiment some grain boundaries had formed a single ledge, some had formed a few and some had formed up to ten. While particle pinning could reduce the grain boundary sliding that caused ledge formation, the orientation of neighboring Sn grains also played a role.

Inspection of a grain boundary region with the maximum of ten grain boundary ledges showed that the grains on either side of the boundary had very different c-axis orientations relative to the sample surface. As shown in the leftmost image in Fig. 6, the c-axis of the right grain was oriented parallel to the sample surface while the c-axis of the left grain was perpendicular to the sample surface. The c-axis orientation was important because the coefficient of thermal expansion (CTE) is twice as high along the c-axis of the Sn lattice than the a-axis. The right grain expanded mostly in the plane of the sample surface, pushing the grain boundary to the left, while the left grain expanded mostly out of the plane, increasing the height of the ledge that formed. This observation is supported by the fact that subsequent grain boundary ledges continued to push the boundary towards the left. The grain boundary sliding and ledge formation occurred due to the stresses induced by the mismatch in CTE of neighboring grains. The overall joint did not experience a change in grain size or texture, indicating that deformation was highly localized around grain boundaries. The mismatch in CTE caused an increase in stress along the grain boundary, triggering diffusion creep processes that

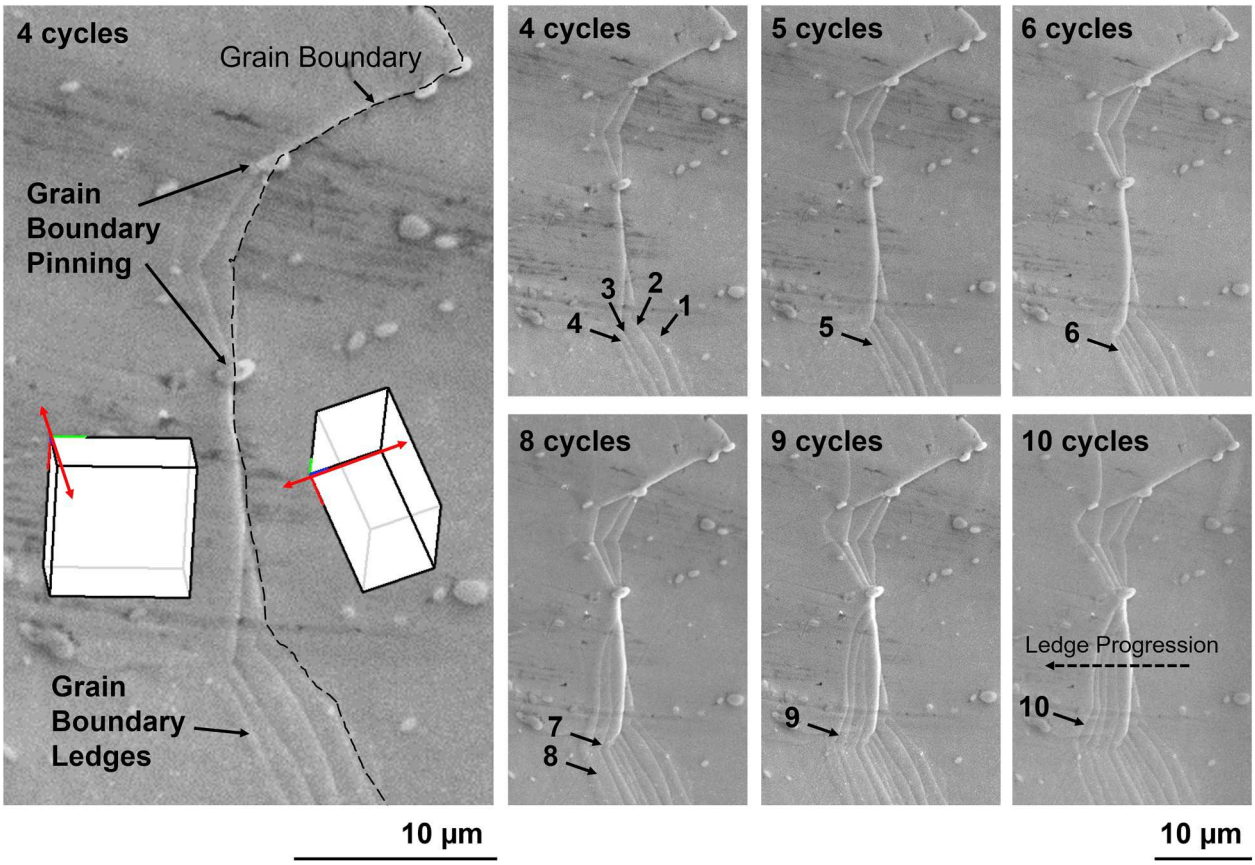

Fig. 6. High resolution SE images of the interrupted thermal aging sample showing the Sn lattices on either side of a grain boundary, grain boundary pinning by fine Cu_6Sn_5 IMC particles and progressive grain boundary ledge formation. The number of grain boundary ledges corresponds to the number of cycles, as shown by the 4 to 6 and 8 to 10 cycle images.

Table 2
Thermal expansion coefficients for Cu, Sn and Cu_6Sn_5 at 150 °C [11].

Material	Coefficient of Thermal Expansion (10^{-6}/K)
Cu	17
βSn	a-axis: 18
	c-axis: 37
Cu_6Sn_5	a-axis: 20
	c-axis: 23

allowed for plastic deformation and stress relief [19,20,22,32]. The formation of ledges was a combination of both grain boundary movement in the plane of the sample surface and normal to the sample surface [33], which occurred due to the c-axis orientation of the grains forming the boundary. In grain pairs with other c-axis relationships the grain boundary between them may have formed a ledge that progressively increased in height or moved in the plane of the sample with no visible surface ledge. The relatively high homologous temperature, 0.43 T_{melt}, fine and randomly oriented grain structure and low strain rate induced by Sn grain CTE mismatch made this an ideal sample to demonstrate grain boundary sliding [34].

After analysis of several time steps it was evident that the number of grain boundary ledges had a one to one correlation with the number of interruptions in the experiment, meaning the ledges had formed during either the heating or cooling step of each interruption. In order to determine when the ledges formed, the interrupted aging sample was compared to the uninterrupted aging sample. The uninterrupted aging sample was imaged after it had been brought to 100 °C and after it had been aged for 120 h, but not cooled to room temperature. As shown in Fig. 2, the uninterrupted aging sample did not show ledge formation. The sample experienced one heating cycle, but no cooling cycle, and the absence of a ledge confirmed that surface ledges form during cooling cycles. It also confirmed that grain boundary sliding and ledge formation was a cyclic process that progressed only with multiple cyclic heating and cooling events.

4.2. *In situ thermal cycling behavior*

The thermally cycled solder joint exhibited significantly greater deformation than either thermally aged sample. The peak temperature in this experiment was 150 °C, greater than half the melting temperature of the solder joint, so grain growth and recrystallization were expected. The higher peak temperature, frequency of cycling and total number of cycles increased the degree of surface damage. As visible in Figs. 4 and 5, the sample showed ledge formation over the entire cross section of the solder joint and there was significant stress relief at the sample surface. This sample degradation was driven by the anisotropic thermal expansion of neighboring Sn grains as discussed in Section 4.1 and thermal expansion of the Cu substrate wires. The CTE characteristics of Cu, βSn and Cu_6Sn_5 are shown in Table 2. The largest thermal expansion occurs along the c-axis of the Sn grain. In the lower temperature thermal aging experiments, grains with the c-axis in the plane of the sample surface caused progressive ledge migration into neighboring grains with their c-axis normal to the sample surface. In the higher temperature thermal cycling experiment, the expansion mismatch between neighboring Sn grains and between the Cu substrate and solder caused much larger ledges to form. The solder region was also compressed along the length of the joint due to the expansion of Cu wires on either side. Upon compression, the more ductile solder bulged outward on its free surfaces, creating the final curved sample surface visible after 118 thermal

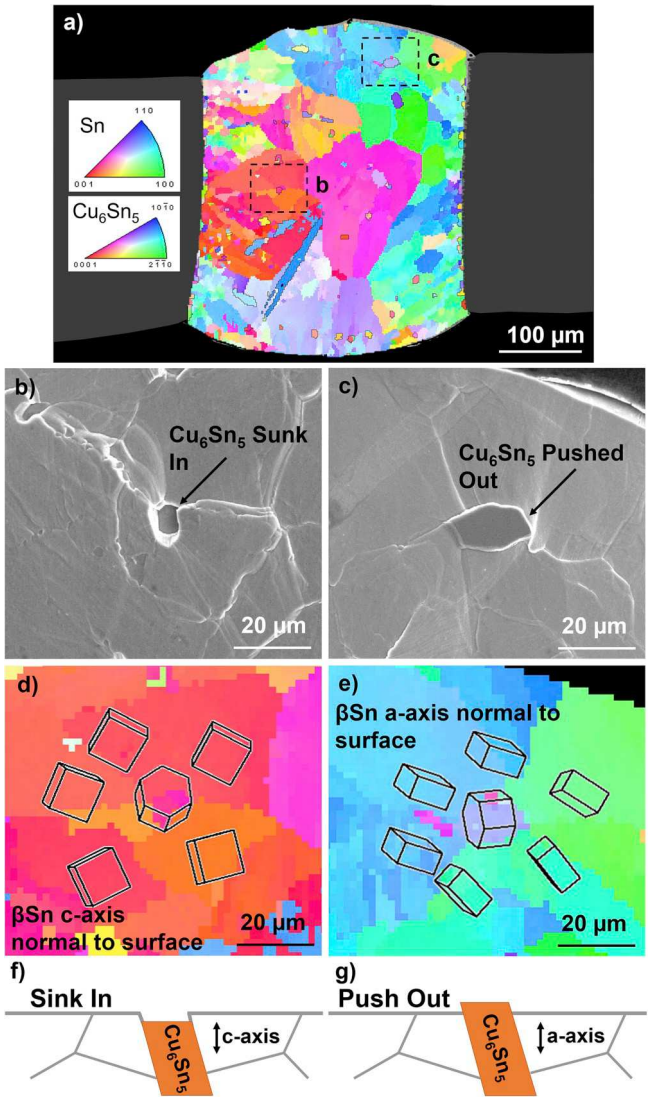

Fig. 7. Investigation of relationship between Sn and Cu_6Sn_5 IMC surface relief: (a) EBSD map of the as-fabricated thermal cycling sample with regions of interest marked in black, (b, c) high resolution SE images of Cu_6Sn_5 IMC needles (b) sunk into and (c) pushed out of the sample surface after 62 cycles, (d,e) OIM maps of (b) and (c) respectively, showing Sn lattices surrounding the Cu_6Sn_5 IMC needle with (d) the c-axis and (e) the a-axis normal to the sample surface, (f,g) schematics showing (f) IMC sink in if the c-axis is normal to the sample surface and (g) IMC push out if a-axis is normal to the sample surface.

cycles. The bulging of the sample surface obscured the interfacial IMC region from view in the SEM, so comments cannot be made about the growth of interfacial IMC. Bulk IMC particles did not exhibit growth or dissolution. As stated in Section 4.1, the short timescale of testing and use of OFHC Cu wires made Kirkendall void formation unlikely.

In addition to the relationship between Sn grains, the relationship between the Cu_6Sn_5 IMC needles and the Sn grains surrounding them was investigated. Two needles from different parts of the solder joint were isolated in high-resolution SEM images, shown in Fig. 7. In one instance, the Sn matrix surrounding the needle had risen, causing the needle to appear sunken into the solder surface. In the second instance, the needle appeared to protrude out of the sample surface. Inspection of the Sn matrix grains revealed that the c-axis orientation controlled the sink-in or push-out characteristic. OIM maps of the two needles, shown in Fig. 7d and e, demonstrate the difference in c-axis orientation. The hexagonal Cu_6Sn_5 IMC has a significantly lower anisotropy than that of Sn, meaning the orientation of the IMC needles did not play a strong role in surface deformation. In the case of the sunken needle, the c-axes of both the Sn matrix and the IMC needle were oriented normal to the sample surface, while in the case of the pushed out needle the a-axis of the Sn matrix was normal to the sample surface and the c-axis of the IMC needle was in the plane of the sample surface. The final part of Fig. 7 schematically illustrates the following process. When the c-axis of the Sn matrix was normal to the sample surface, the Sn expanded more than the IMC needle because the CTE along the c-axis of Sn is 38% greater than that along the c-axis of the IMC. The matrix expanded more than the needles, making the needle appear sunken into the sample surface. When the a-axis of the Sn matrix was normal to the sample surface, the IMC needle expanded more than the Sn because the CTE along the a-axis of Sn is 10% less than that along the a-axis of the IMC. In this case, the needle expanded more than the Sn matrix and protruded from the sample surface.

5. Conclusions

A methodology for investigating *in situ* thermomechanical damage evolution was presented. An *in situ* fixture was utilized to study microstructural evolution such as tin grain growth and grain boundary ledge formation. Thermal aging at 100 °C for 120 h was conducted on a 500 μm solder joint with interruptions for SEM analysis. One predominant damage feature was observed. Grain boundary sliding and anisotropic thermal expansion of neighboring Sn grains created raised ledges along high angle grain boundaries. Grain rotation and growth were not observed due to the low aging temperature. In order to determine when grain boundary ledges formed, an uninterrupted aging test was conducted at the same temperature and for the same duration but was imaged prior to cooling to room temperature. To study the influence of temperature on observed damage phenomena, thermal cycling was done on a similar solder joint, cycled between room temperature and 150 °C with a cycle time of 1 h for a total of 118 cycles. Grain boundary ledges and surface relief were present over the entire sample cross section and the solder region was compressed due to thermal expansion of the Cu wires. The following conclusions were drawn from this work.

1. Ledges formed along high angle grain boundaries and could be pinned by fine Cu_6Sn_5 IMC particles. In IMC particle-free regions, grain boundary ledges formed to expand Sn grains with their c-axis in the plane of the sample surface and shrink grains with their c-axis normal to the sample surface.
2. Grain boundary ledges formed during the cooling cycle of thermal experiments.
3. IMC needles appeared both sunken into and protruding from the sample surface, due to the difference in CTE between the needles and the surrounding Sn matrix. When the c-axis of the Sn matrix was normal to the sample surface, the Sn expanded more than the IMC, making the needles appear sunken. When the a-axis of the Sn matrix was normal to the sample surface, the IMC needles expanded more than the Sn, making the needles protrude from the surface.

Declaration of competing interest

The authors declare that they have no known competing financial interests or personal relationships that could have appeared to influence the work reported in this paper.

Acknowledgements

The authors gratefully acknowledge financial support from the Semiconductor Research Corporation (Dr. John Candelaria, program manager) and the facilities at the LeRoy Eyring Center for Solid State Sciences at Arizona State University. This work was also supported by the National Science Foundation under grant NSF CMMI-1763128 (Dr. Alexis Lewis, Program Manager).

References

[1] S. Kang, A. Sarkhel, Lead (Pb)-free solders for electronic packaging, J. Electron. Mater. 23 (8) (1994).
[2] E. Wood, K. Nimmo, In search of new lead-free electronic solders, J. Electron. Mater. 23 (8) (1994).
[3] N. Jiang, J.A. Clum, R.R. Chromik, E.J. Cotts, Thermal expansion of several Sn-based intermetallic compounds, Scr. Mater. 37 (12) (1997).
[4] K.N. Subramanian, J.G. Lee, Effects of internal stresses on the thermomechanical behavior of Sn-based solder joints, Mater. Sci. Eng. A 421 (2006) 46–56.
[5] B. Dyson, T. Anthony, D. Turnbull, Interstitial diffusion of copper in tin, J. Appl. Phys. 38 (8) (1967), 3408-3408.
[6] B.F. Dyson, Diffusion of gold and silver in tin single crystals, J. Appl. Phys. 37 (6) (1966) 2375–2377.
[7] D. Yeh, H. Huntington, Extreme fast-diffusion system: nickel in single-crystal tin, Phys. Rev. Lett. 53 (15) (1984) 1469.
[8] T. Bieler, H. Jiang, L. Lehman, T. Kirkpatrick, E. Cotts, Influence of Sn Grain Size and Orientation on the Thermomechanical Response and Reliability of Pb-free Solder Joints. 56th Electronic Components and Technology Conference, IEEE, 2006.
[9] M. Lu, D.-Y. Shih, P. Lauro, C. Goldsmith, D.W. Henderson, Effect of Sn grain orientation on electromigration degradation mechanism in high Sn-based Pb-free solders, Appl. Phys. Lett. 92 (21) (2008), 211909.
[10] J. Sylvestre, A. Blander, Large-scale correlations in the orientation of grains in lead-free solder joints, J. Electron. Mater. 37 (10) (2008) 1618–1623.
[11] J.W. Xian, G. Zeng, S.A. Belyakov, Q. Gu, K. Nogita, C.M. Gourlay, Anisotropic thermal expansion of Ni_3Sn_4, Ag_3Sn, Cu_3Sn, Cu_6Sn_5 and βSn, Intermetallics 91 (2017) 50–64.
[12] T.R. Bieler, B. Zhou, L. Blair, A. Zamiri, P. Darbandi, F. Pourboghrat, T.-K. Lee, K.-C. Liu, The role of elastic and plastic anisotropy of Sn in recrystallization and damage evolution during thermal cycling in SAC305 solder joints, J. Electon. Mater. 41 (2) (2012).
[13] H. Chen, L. Wang, J. Han, M. Lu, H. Liu, Microstructure, orientation and damage evolution in SnPb, SnAgCu, and mixed solder interconnects under thermomechanical stress, Microelectron. Eng. 96 (2012) 82–91.
[14] R.D. Doherty, D.A. Hughes, F.J. Humphreys, J.J. Jonas, D. Juul Jensen, M. E. Kassner, W.E. King, T.R. McNelley, H.J. McQueen, A.D. Rollett, Current issues in recrystallization: a review, Mater. Sci. Eng. A 238 (1997) 219–274.
[15] J.J. Sundelin, S.T. Nurmi, T.K. Lepisto, Recrystallization behaviour of SnAgCu solder joints, Mater. Sci. Eng. A 474 (2008) 201–207.
[16] J. Han, F. Guo, J.P. Liu, Early stages of localized recrystallization in Pb-free BGA solder joints subjected to thermomechanical stress, J. Alloy. Comp. 704 (2017) 574–584.
[17] G. Liu, S. Ji, Microstructure, dynamic restoration and recrystallization texture of Sn-Cu after rolling at room temperature, Mater. Char. 150 (2019) 174–183.
[18] L. Yin, L. Wentlent, L. Yang, B. Arfaei, A. Oasaimeh, P. Borgesen, Recrystallization and precipitate coarsening in Pb-free solder joints during thermomechanical fatigue, J. Electron. Mater. 41 (2) (2012).
[19] M.A. Matin, W.P. Vellinga, M.G.D. Geers, Thermomechanical fatigue damage evolution in SAC solder joints, Mater. Sci. Eng. A 445 (2007) 73–85.
[20] A.U. Telang, T.R. Bieler, A. Zamiri, F. Pourboghrat, Incremental recrystallization/grain growth driven by elastic strain energy release in a thermomechanically fatigued lead-free solder joint, Acta Mater. 55 (7) (2007) 2265–2277.
[21] H. Chen, J. Han, M. Li, Localized recrystallization induced by subgrain rotation in Sn-3.0 Ag-0.5 Cu ball grid array solder interconnects during thermal cycling, J. Electron. Mater. 40 (12) (2011) 2470–2479.
[22] B. Zhou, Q. Zhou, T.R. Bieler, T.K. Lee, Slip, crystal orientation, and damage evolution during thermal cycling in high-strain wafer-level chip-scale packages, J. Electron. Mater. 44 (3) (2015) 895–908.
[23] J.C. Mertens, A. Kirubanandham, N. Chawla, In situ fixture for multi-modal characterization during electromigration and thermal testing of wire-like microscale specimens, Microelectron. Reliab. 55 (11) (2015) 2345–2353.
[24] J.C.E. Mertens, A. Kirubanadham, N. Chawla, Electromigration mechanisms in Sn-0.7Cu/Cu couples by four dimensional (4D) X-ray microtomography and electron backscatter diffraction (EBSD), Acta Mater. 102 (2016) 220–230.
[25] A. Kirubanandham, I. Lujan-Regalado, R. Vallabhaneni, N. Chawla, Three dimensional characterization of tin crystallography and Cu_6Sn_5 intermetallics in solder joints by multiscale tomography, JOM 68 (11) (2016) 2879–2887.
[26] L. Yin, P. Borgesen, On the root cause of Kirkendall voiding in Cu_3Sn, J. Mater. Res. 26 (3) (2011).
[27] M. He, A. Kumar, P.T. Yeo, G.J. Qi, Z. Chen, Interfacial reaction between Sn-rich solders and Ni-based metallization, Thin Solid Films 462–463 (2004) 387–394.
[28] B. Chao, S.-H. Chae, X. Zhang, K.-H. Lu, J. Im, P.S. Ho, Investigation of diffusion and electromigration parameters for Cu-Sn intermetallic compounds in Pb-free solders using simulated annealing, Acta Mater. 55 (2007) 2805–2814.
[29] T. Laurila, V. Vuorinen, J.K. Kivilahti, Interfacial reactions between lead-free solders and common base materials, Mater. Sci. Eng. R Rep. R 49 (2005) 1–60.
[30] M. Kerr, N. Chawla, Creep deformation behavior of Sn-3.5Ag solder/Cu couple at small length scales, Acta Mater. 52 (2004) 4527–4535.
[31] F. Ochoa, X. Deng, N. Chawla, Effects of cooling rate on creep behavior of Sn-3.5Ag alloy, J. Electron. Mater. 33 (12) (2004) 1596–1607.
[32] M.A. Matin, E.W.C. Coenen, W.P. Vellinga, M.G.D. Geers, Correlation between thermal fatigue and thermal anisotropy in a Pb-free solder alloy, Scr. Mater. 53 (2005) 927–932.
[33] K.N. Subramanian, J.G. Lee, Effect of anisotropy of tin on thermomechanical behavior of solder joints, J. Mater. Sci. Mater. Electron. 15 (2004) 235–240.
[34] Q.K. Zhang, Z.F. Zhang, In situ observations on shear and creep-fatigue fracture behaviors of SnBi/Cu solder joints, Mater. Sci. Eng. A 528 (2011) 2686–2693.